Calculations of Velocity-Scalar Joint pdf's

S.B. Pope

Massachusetts Institute of Technology, Department of Mechanical Engineering,
Cambridge, MA 02139, USA

Abstract

A joint pdf transport equation has been solved to calculate the properties of the self-similar, plane, turbulent jet. The joint probability density function (pdf) is that of the three velocity components and of the nozzle-fluid concentration, which is a conserved, passive scalar. The advantage of basing a turbulence closure on the joint pdf equation is that convective transport appears in closed form. Consequently, the gradient-diffusion assumption is avoided. For self-similar shear flows, the joint pdf is a function of five variables. Its transport equation is solved by a Lagrangian method with stochastic modelling of the unclosed terms. The calculated Reynolds stresses and triple velocity correlations agree well with the experimental data. Calculated pdf's and joint pdf's are also reported.

Nomenclature

C_R, C_ϕ	model constants
D	velocity dissipation term
E	conditionally-expected value
$f(V,\psi)$	velocity-scalar joint pdf
G	scalar dissipation term
$p(\psi)$	scalar pdf
$<p>, p'$	mean and fluctuating pressure
R	redistribution term
r, θ, z	polar-cylindrical coordinates
$t, \Delta t$	time, time interval
$\boldsymbol{U}, \boldsymbol{u}$	velocity, fluctuating velocity
$\boldsymbol{V}$	independent velocity variables
x, y, z	axial, lateral and spanwise coordinates
$y_{1/2}$	jet half width

Greek Symbols

Γ	molecular diffusion coefficient
ϵ	dissipation rate of turbulent kinetic energy
η	cross-stream variable $y/y_{1/2}$
μ	molecular viscosity
ϕ, ϕ'	scalar, fluctuating scalar
ψ	independent scalar variable
ω, ω^*	turbulent frequency, normalised frequency

Introduction

A modelled joint pdf equation [1] has been solved to calculate the one-point statistical properties of the self-similar plane turbulent jet. The equation solved is for the joint prob-

---

Permanent address: Cornell University, Mechanical and Aerospace Engineering, Ithaca NY 14853, USA

ability density function (pdf) of the three velocity components $\boldsymbol{U}(\boldsymbol{x},t)$ and a conserved passive scalar $\phi(\boldsymbol{x},t)$. With θ being the non-dimensional, cross-stream variable, the joint pdf is $f(V,\psi;\theta)$, where $V \equiv V_1$, V_2, V_3 and ψ are the independent variables corresponding to $\boldsymbol{U}$ and ϕ. Since $f(V,\psi;\theta)$ is a function of five variables, the solution of its transport equation by a finite-difference method is impracticable. Instead, the transport equation is solved by a Lagrangian method with stochastic modelling of the unclosed terms. The simplest possible models are used – not the most accurate – the emphasis being on demonstrating the use of the joint pdf equation and the performance of the solution procedure.

Transport equations for pdf's are useful in modelling turbulent flows because non-linear one-point processes (such as convection and reaction) can be treated without approximation [1–3]. The transport equation for the joint pdf of a set of scalars $p(\psi;\boldsymbol{x},t)$ is particularly useful in reactive flows since the term pertaining to reaction appears in closed form, irrespective of the complexity and non-linearity of the reaction scheme. *Pope* [4] and *Janicka* et al. [5] have reported accurate calculations of premixed and diffusion flames based on the scalar pdf equation. For more than one or two scalars, finite-difference solutions are impracticable, but a Monte Carlo method [6] has been developed for the general case.

The great advantage of considering the joint pdf of velocity and scalars is that convective transport appears in closed form. Consequently, the assumption of turbulent transport by gradient diffusion is avoided. In fact, for a variable-density reactive flow, the terms pertaining to convection, reaction, buoyancy and the mean pressure gradient all appear in closed form. Only the effects of molecular mixing and the fluctuating pressure gradient need to be modelled. Models for these processes have been given in a recent paper [1] which contains a derivation and discussion of the joint pdf equation.

Self-similar free shear flows are good test cases for the modelled joint pdf equation. The condition of self-similarity can be used to reduce the number of spatial dimensions to one – namely, the normalized cross-stream coordinate θ. And for self-similar flows there is a wealth of experimental data. The plane jet was chosen for this initial study because of the simple coordinate system and boundary conditions.

In the following three sections, the joint pdf transport equation is presented, the solution procedure is described, and the results of the calculations are reported. The results include profiles of the mean velocity, Reynolds stresses and triple velocity correlations, all of which are compared with the experimental data of *Heskestad* [7]. Calculated scalar pdf's and joint pdf's are also reported but no data are available for comparison.

Joint pdf Equation

The joint pdf $f(V,\psi;\boldsymbol{x},t)$ contains all the one-point statistical information about the velocity $\boldsymbol{U}(\boldsymbol{x},t)$ and the conserved, passive scalar $\phi(\boldsymbol{x},t)$ in a constant-density turbulent flow. If $Q(\boldsymbol{U},\phi)$ is any function of $\boldsymbol{U}$ and ϕ, then its mean value (at any $\boldsymbol{x},t$) can be determined from the joint pdf by

$$<Q(\boldsymbol{U},\phi)> = \int\int Q(V,\psi)\, f(V,\psi)\, dV\, d\psi \quad . \tag{1}$$

Here and below, $\int dV$ represents integration over the whole of the velocity space and, similarly, $\int d\psi$ represents integration over all possible values of ϕ. Substituting $Q(\boldsymbol{U},\phi) = U_j$ in Eq. (1) shows the mean velocity to be

$$<U_j> = \int\int V_j f(\boldsymbol{V},\psi)\, dV\, d\psi \quad . \tag{2}$$

Similarly the Reynolds stresses are

$$<u_i u_j> = \int\int (V_i - <U_i>)\,(V_j - <U_j>)\, f(\boldsymbol{V},\psi)\, dV\, d\psi \quad , \tag{3}$$

and the scalar fluxes are

$$<u_i \phi'> = \int\int (V_i - <U_i>)\,(\psi - <\phi>)\, f(\boldsymbol{V},\psi)\, dV\, d\psi \quad . \tag{4}$$

Thus, any one-point statistic can be obtained from $f(\boldsymbol{V},\psi)$.

The pdf of the scalar alone $p(\psi;\boldsymbol{x},t)$ is obtained by integrating $f(\boldsymbol{V},\psi)$ over velocity space

$$p(\psi) = \int f(\boldsymbol{V},\psi)\, dV \quad , \tag{5}$$

and the joint pdf of velocity $g(\boldsymbol{V};\boldsymbol{x},t)$ is

$$g(\boldsymbol{V}) = \int f(\boldsymbol{V},\psi)\, d\psi \quad . \tag{6}$$

Each of the pdf's satisfies the normalization condition

$$\int p(\psi)\, d\psi = \int g(\boldsymbol{V})\, dV = \int\int f(\boldsymbol{V},\psi)\, dV\, d\psi = 1 \quad . \tag{7}$$

A transport equation for $f(\boldsymbol{V},\psi;\boldsymbol{x},t)$ can be derived from the conservation equations for $\boldsymbol{U}$ and ϕ [1]:

$$\frac{\partial f}{\partial t} + V_i \frac{\partial f}{\partial x_i} - \frac{\partial f}{\partial V_i}\frac{\partial <p>}{\partial x_i} = \frac{\partial}{\partial V_j}\left[f\,\mathrm{E}(\partial p'/\partial x_j \,|\, \boldsymbol{U} = \boldsymbol{V}, \phi = \psi)\right]$$

$$- \frac{\partial}{\partial V_j}\left[f\,\mathrm{E}(\mu \nabla^2 U_j \,|\, \boldsymbol{U} = \boldsymbol{V}, \phi = \psi)\right]$$

$$- \frac{\partial}{\partial \psi}\left[f\,\mathrm{E}(\Gamma \nabla^2 \phi \,|\, \boldsymbol{U} = \boldsymbol{V}, \phi = \psi)\right] \quad . \tag{8}$$

(The fluid density ρ has been set to unity.) The terms on the left-hand side represent convection and the effect of the mean pressure gradient. These terms are in closed form and therefore require no modelling. The terms on the right-hand side of the equation contain (as unknowns to be modelled) conditionally-expected values.

The first term on the right-hand side

$$R(\boldsymbol{V},\psi;\boldsymbol{x},t) = \frac{\partial}{\partial V_j}\left[f\mathrm{E}(\partial p'/\partial x_j \,|\, \boldsymbol{U} = \boldsymbol{V}, \phi = \psi)\right] \quad , \tag{9}$$

represents the effects of the fluctuating pressure gradient. The term can be decomposed into three parts [1]: a transport term and two redistribution terms. As in Reynolds-stress models [8], the redistribution terms do not affect the mean velocity or the turbulent kinetic energy, but they redistribute the energy in velocity space. The *rapid* part of the redistribution is due to pressure fluctuations caused by mean-velocity gradients: the *Rotta* part [9] is due solely to the turbulence. Models for all three contributions to

$R(V,\psi;x,t)$ are available [1], but for this initial study only the Rotta term is included.

In Reynolds-stress models, the Rotta term corresponds to a linear return to isotropy, i.e.

$$\frac{\partial}{\partial t}<u_i u_j> = \ldots - C_R\,\omega(<u_i u_j> - 1/3\,<u_l u_l>\,\delta_{ij}) \quad , \tag{10}$$

where C_R is a constant and $\omega(x,t)$ is the turbulent frequency (dissipation rate/turbulent kinetic energy). In the joint pdf equation, this term is modelled by a stochastic process that randomly reorientates the energy in velocity space. The effect on the Reynolds stresses is just that given by Eq. (10).

The second term on the right-hand side of Eq. (8)

$$D(V,\psi;x,t) = -\frac{\partial}{\partial V_j}\,[f\,\mathrm{E}(\mu\nabla^2 U_j \,|\, U = V, \phi = \psi)] \quad , \tag{11}$$

corresponds to dissipation – it does not affect the mean velocity but decreases the turbulent kinetic energy. Neglecting low-Reynolds-number terms, D is related to the dissipation [1] by

$$\epsilon = \int\int 1/2\;\; V_i\;\; V_i\;\; D(V,\psi;x,t)\,dV\,d\psi \quad . \tag{12}$$

In the joint pdf equation, *Curl*'s coalescence/dispersal model [10] is used to represent this process. (Because the turbulent frequency ω is defined in terms of ϵ, no additional model constant arises).

The final term in Eq. (8)

$$G(V,\psi;x,t) = -\frac{\partial}{\partial \psi}\,[f\,\mathrm{E}(\Gamma\nabla^2\phi \,|\, U = V, \phi = \psi)] \quad , \tag{13}$$

corresponds to scalar dissipation and is analogous to the velocity dissipation term D. The effect of the term is to reduce the scalar variance $<\phi'^2>$ without affecting the mean $<\phi>$. Again, *Curl*'s model [10] is used to represent the process. The model involves a constant C_ϕ which is the ratio of the velocity to scalar turbulent time scales. Following conventional modelling [11] we take $C_\phi = 2.0$.

The calculations for the self-similar plane jet are performed in the polar-cylindrical coordinates r, θ, z. The distance from the virtual origin is r, the angle to the plane of symmetry is θ, and z is the spanwise distance. Some of the results are reported in the conventional Cartesian coordinate system (x,y,z) in which x is the axial distance ($x = r\cos\theta$) and y is the lateral distance ($y = r\sin\theta$). The half-width of the jet is $y_{1/2}$. It is assumed that the turbulent frequency $\omega(r,\theta,z)$ does not vary across the jet – i.e. that ω is independent of θ. Then, the conditions for self-similarity require that the normalized frequency

$$\omega^* \equiv \omega y_{1/2} \,/\, <U>_0 \quad , \tag{14}$$

be a constant. ($<U>_0$ is the center-line velocity.) By transforming Eq. (8) into polar-cylindrical coordinates and applying the conditions of self-similarity, a transport equation is obtained for the joint pdf $f(V_r, V_\theta, V_z, \psi;\theta,t)$. This equation is obtained without invoking the boundary-layer assumptions and without neglecting any terms. It is solved for $0 \leqslant \theta \leqslant \theta_{max} = 0.5$, with symmetry conditions applied at $\theta = 0$ and with the boundary conditions at θ_{max} corresponding to potential flow with $\phi = 0$.

The values of the constants $\omega^* = 0.165$ and $C_R = 4.5$ are chosen to produce approximately the correct spreading rate ($dy_{1/2}/dx \cong 0.1$) and center-line turbulent kinetic energy ($1/2 \langle u_i u_i \rangle_0 / \langle U \rangle_0^2 \cong 0.065$). The value of C_R is greater than the usual value $C_R = 1.5$ [8] because the modelled redistribution term has to account for both the Rotta and rapid terms.

To summarize, in the joint pdf equation, Eq. (8), convective transport appears in closed form. Consequently, there are no Reynolds stresses, scalar fluxes or other velocity correlations to be modelled: the gradient-transport assumption is avoided. There are three unclosed terms representing, respectively, redistribution of kinetic energy in velocity space, dissipation of velocity fluctuations, and dissipation of scalar fluctuations. These three terms are modelled by simple stochastic processes, each of which proceeds at a rate proportional to the turbulent frequency ω. For the self-similar plane jet, the turbulent frequency is assumed to be uniform across the jet. A fuller description and analytic expressions for the models can be found in [1].

Solution Procedure

Since the joint pdf $f(V_r, V_\theta, V_z, \psi; \theta, t)$ is a function of five independent variables and time, it is obvious that its transport equation cannot be solved by a standard numerical method. The solution is obtained as the steady state of a transient calculation. The calculation advances from time t to time $t + \Delta t$ in two fractional steps. In the first step, the exact terms are treated by solving the equation

$$\frac{\partial f}{\partial t} + V_i \frac{\partial f}{\partial x_i} - \frac{\partial f}{\partial V_i} \frac{\partial \langle p \rangle}{\partial x_i} = 0 \quad , \tag{15}$$

by a Lagrangian method. In the second step, stochastic models are used to solve the equation

$$\frac{\partial f}{\partial t} = R + D + G \quad . \tag{16}$$

After the second step, the result is the pdf at time $t + \Delta t$ (according to Eq. 8) plus a truncation error of order Δt^2. The truncation error can be reduced at will by reducing Δt.

In the numerical procedure, the pdf is represented indirectly by a large number (N) of elements in the solution domain $0 \leqslant \theta \leqslant \theta_{max} = 0.5$. The nth element is located at $\theta^{(n)}$ and has the properties $U_r^{(n)}$, $U_\theta^{(n)}$, $U_z^{(n)}$, $\phi^{(n)}$. The elements are approximately uniformly distributed. Consequently, the number M of elements in the small sub-interval $\theta - 1/2\Delta\theta < \theta^{(n)} \leqslant \theta + 1/2\Delta\theta$ is

$$M \approx \Delta\theta N / \theta_{max} \quad , \tag{17}$$

Let $n_1, n_2, \ldots, n_M$ be the M elements in the sub-interval. Then, at location θ, an approximation to the mean of any function $Q(\boldsymbol{U}, \phi)$ is

$$\langle Q(\boldsymbol{U}, \phi) \rangle \cong \frac{1}{M} \sum_{m=1}^{M} Q(\boldsymbol{u}^{(n_m)}, \phi^{(n_m)}) \quad . \tag{18}$$

Similarly, the joint pdf at θ can be approximated by the histogram formed from the M elements.

In the approximation of the mean, Eq. (18), there is a truncation error (of order $\Delta\theta^2$) and a statistical sampling error of order $M^{-1/2}$. These errors can, in principle, be reduced at will by decreasing $\Delta\theta$ and increasing $N\Delta\theta$. In practice, for realistic values of N and $\Delta\theta$, the error is large, and a more sophisticated method of determining means based on least-square cubic splines is used. But the principle is the same.

The solution of Eq. (15) is facilitated by the observation that it is the pdf transport equation for the Lagrangian system:

$$\frac{dx}{dt} = U \quad , \quad \frac{dU}{dt} = -\nabla <p> \quad , \quad \frac{d\phi}{dt} = 0 \quad . \tag{19}$$

Thus, for the first of the fractional steps, the properties of each of the N elements evolve according to Eq. (19) for a time Δt.

In the second fractional step, stochastic models are used to solve Eq. (16). Pairs of elements that are close to each other in physical space interact to cause redistribution and velocity and scalar dissipation – the terms R, D and G. The solution domain is divided into K sub-intervals, of width $\Delta\theta = \theta_{max}/K$, and the ensembles of elements within each sub-interval are treated separately.

In Curl's model for the velocity dissipation (D), each ensemble is treated in turn and the following procedure is repeated n_D times, where

$$n_D = \omega \Delta t M \quad . \tag{20}$$

Two elements, denoted by n and m, are selected at random from the ensemble, and their velocities are replaced with the values

$$U^{(n)} = U^{(m)} = 1/2\,(U_0^{(n)} + U_0^{(m)}) \quad , \tag{21}$$

where $U_0^{(n)}$ is the value of $U^{(n)}$ before the process. This has the effect of decreasing the energy $<U \cdot U>$ without affecting the mean $<U>$.

The implementation of Curl's model for the scalar dissipation (G) is precisely analogous. A pair of elements (n and m) is selected at random and the values of ϕ are replaced with

$$\phi^{(n)} = \phi^{(m)} = 1/2\,(\phi_0^{(n)} + \phi_0^{(m)}) \quad . \tag{22}$$

This process is repeated

$$n_G = C_\phi\, \omega \Delta t M \quad , \tag{23}$$

times, which has the effect of decreasing the scalar variance $<\phi'^2>$ without affecting the mean $<\phi>$.

In the stochastic model of redistribution (R), a pair of elements is selected at random from the ensemble. The velocities of the two elements (n and m) are then replaced with the values

$$U^{(n)} = 1/2\,(U_0^{(n)} + U_0^{(m)}) + 1/2\,\xi |\, U_0^{(n)} - U_0^{(m)} |\quad , \tag{24}$$

and

$$U^{(m)} = 1/2\,(U_0^{(n)} + U_0^{(m)}) - 1/2\,\xi |\, U_0^{(n)} - U_0^{(m)} |\quad , \tag{25}$$

where ξ is a random vector of unit length, uniformly distributed on the unit sphere. This transformation from $U_0^{(n)}$, $U_0^{(m)}$ to $U^{(n)}$, $U^{(m)}$ corresponds to a random rotation of the elements in velocity space. Since neither their mean position nor their separation is altered, the transformation conserves both momentum and energy; the effect of the random rotation is to decrease the anisotropy.

This process is repeated n_R times, where

$$n_R = C_R \, \omega \Delta t M \quad . \tag{26}$$

The two fractional steps advance time by Δt. Starting from a specified initial condition, this sequence of operations is repeated until the statistically steady state is reached. The steady state is independent of the initial condition.

For the calculations reported in the next section, there were N = 7,200 elements, and K = 48 sub-intervals in the solution domain $0 \leqslant \theta \leqslant \theta_{max} = 0.5$. With a time step of $\Delta t = 0.2 y_{1/2} / <U>_0$, 400 time steps were taken. (The sampling error is decreased by time-averaging: hence the large number of steps). The total CPU time on a VAX computer was 27 min, at a cost of $ 16.

Results

The calculations reported in this section were obtained from the numerical solution of the modelled joint pdf equation. Calculated profiles of mean velocity, Reynolds stresses and triple correlations are compared with the hot-wire data of *Heskestad* [7]. Scalar pdf's and a joint velocity pdf are also reported, but there are no data for comparison. All the results are normalised with the center-line values $<U_0>$ and $<\phi_0>$.

Figure 1 shows the mean axial velocity profile. Although the calculations are performed in polar-cylindrical coordinates, the results are transformed to cartesian coordinates for comparison with the data. Thus Fig. 1 shows the mean velocity in the x-direction against the normalised y-coordinate,

$$\eta \equiv y / y_{1/2} \quad . \tag{27}$$

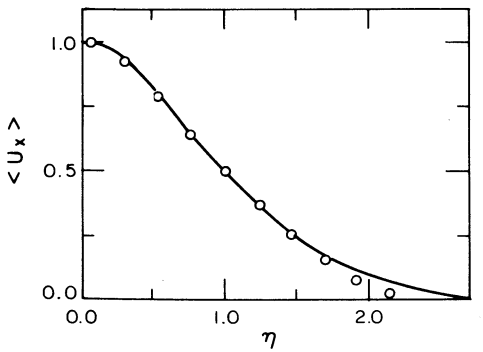

Fig. 1. Mean axial velocity against lateral distance: (——) calculation; (○) experiment [7]

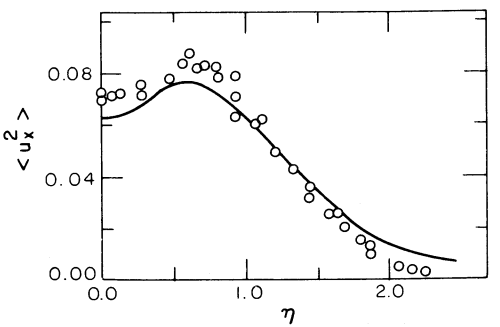

Fig. 2. Mean square axial velocity fluctuations against lateral distance: (——) calculation; (○) experiment [7]

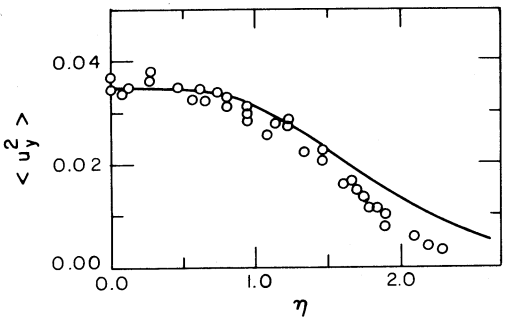

Fig. 3. Mean square lateral velocity fluctuations against lateral distance: (——) calculation; (○) experiment [7]

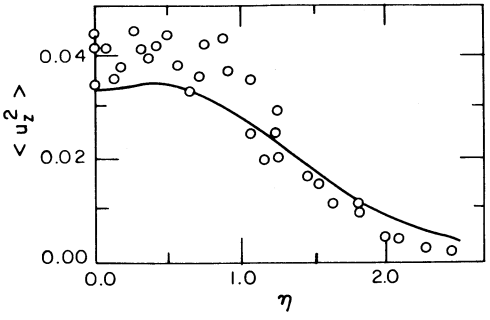

Fig. 4. Mean square spanwise velocity fluctuations against lateral distance: (——) calculation; (○) experiment [7]

There is good agreement between the calculated and measured profiles, but it should be remembered that the normalisation forces agreement at $\eta = 0$ and $\eta = 1$.

Figures 2–4 show the normal stress profiles $<u_x^2>$, $<u_y^2>$ and $<u_z^2>$. The profile shapes are calculated quite accurately as are the relative magnitudes, i.e.

$$<u_x^2> \approx 2<u_y^2> \approx 2<u_z^2> \quad . \tag{28}$$

It may be recalled that the constants ω^* and C_R were chosen so that the calculated spreading rate and the center-line kinetic energy agree with the measured values. It is not completely surprising, therefore, that the magnitude of the calculated normal stresses agrees well with the data. One feature of interest is the maximum in $<u_x^2>$ away from the plane of symmetry. This occurs because the production of $<u_x^2>$ is relatively small at $\eta = 0$.

Profiles of the shear stress $<u_x u_y>$ are shown in Fig. 5. It may be seen that the measured values are, typically, 20% lower than the calculations. Using the measured

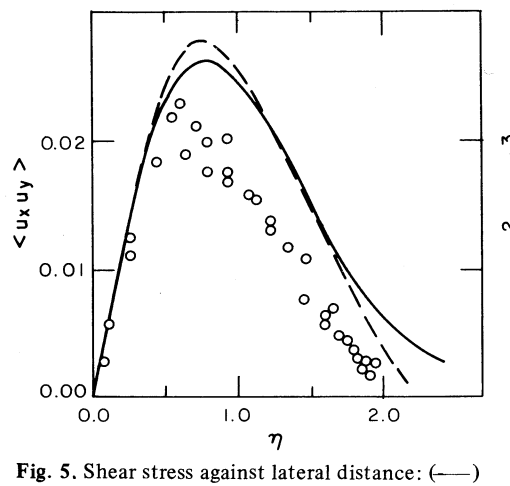

Fig. 5. Shear stress against lateral distance: (——) calculation; (○) experiment [7]; (– – –) deduced from measured mean velocity and momentum balance [7]

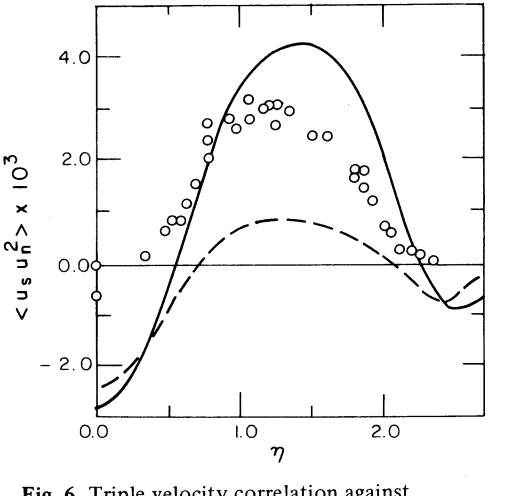

Fig. 6. Triple velocity correlation against lateral distance: (——) calculation; (○) experiment [7]; (– – –) gradient model [8] evaluated from calculated Reynolds stresses

mean velocity and normal stresses, Heskestad used the axial momentum equation to obtain an independent estimate of the shear stresses. This estimate (indicated by the broken line) is in good agreement with the calculation. This supports Heskestad's conclusion that the measured values of $\langle u_x u_y \rangle$ are subject to error.

Heskestad's results include triple velocity correlations, measured in a local mean-streamline coordinate system. In the x-y plane, the fluctuating velocity components parallel and normal to the mean velocity vector are u_s and u_n. Figure 6 shows measured and calculated values of the triple correlation $\langle u_s u_n^2 \rangle$. Also shown on the figure is the value of the triple correlation obtained from Launder, Reece and Rodi's [8] gradient diffusion model

$$\langle u_i u_j u_k \rangle = -\frac{0.11}{\omega} \langle u_i u_l \rangle \frac{\partial}{\partial x_l} \langle u_j u_k \rangle + \langle u_j u_l \rangle \frac{\partial}{\partial x_l} \langle u_k u_i \rangle + \langle u_k u_l \rangle \frac{\partial}{\partial x_l} \langle u_i u_j \rangle \quad (29)$$

Near to the plane of symmetry $0 \leqslant \eta \leqslant 0.5$, both the joint-pdf calculations and the gradient model give significant negative values, while the measured values are close to zero. The maximum value of $\langle u_s u_n^2 \rangle$ occurs at $\eta \approx 1$: the maximum value from the joint pdf calculation is 30% greater than that measured, while for the gradient model it is 80% less. The level of agreement between the measurements and the joint-pdf calculations is satisfactory considering the likely measurement error and the simplicity of the closure assumptions.

This completes the comparison of calculated velocity statistics with the experimental data of Heskestad. For the scalar field, the only measurements are for the mean profile, see [12] for example. It is found that for the self-similar plane jet, the spreading rate of the mean scalar is 40% greater than the spreading rate of the mean velocity. In the calculations, however, the scalar spreading rate is 5% less. This disappointing result is undoubtedly due to the simplistic modelling of the fluctuating pressure gradient terms. Future calculations that include the rapid term and the pressure transport term will, hopefully, not suffer from this defect. The normalised profile (not shown) is calculated accurately.

Some pdf's are now reported to illustrate the type of quantities that can be calculated. Figure 7 shows the scalar pdf $p(\psi)$

$$p(\psi) = \int f(V, \psi)\, dV \quad , \quad (30)$$

for different values of η. On the plane of symmetry ($\eta = 0$), the pdf is a bell-shaped curve and some negative skewness is evident. At $\eta = 0.5$ the pdf has the same shape but the mean is shifted to a lower value and the standard deviation is increased. At $\eta = 1.0$, the effect of the lower bound becomes evident. That is, the minimum possible value of ϕ is zero, and hence the pdf is zero for negative values of ψ. As can be seen from the figure, this leads to a discontinuity in $p(\psi)$ at $\psi = 0$. At the furthest location shown, $\eta = 1.5$, the pdf is centered on low values of ψ, corresponding to recently entrained fluid.

Also shown on Fig. 7 are the contributions to $p(\psi)$ of outward flowing fluid. The scalar pdf can be decomposed into two parts

$$p(\psi) = p_+(\psi) + p_-(\psi) \quad , \quad (31)$$

where

$$p_+(\psi) = \int_{-\infty}^{\infty} \int_{0}^{\infty} \int_{-\infty}^{\infty} f(V_r, V_\theta, V_z, \psi)\, dV_r\, dV_\theta\, dV_z \quad , \tag{32}$$

and

$$p_-(\psi) = \int_{-\infty}^{\infty} \int_{-\infty}^{0} \int_{-\infty}^{\infty} f(V_r, V_\theta, V_z, \psi)\, dV_r\, dV_\theta\, dV_z \quad . \tag{33}$$

The contribution to $p(\psi)$ from outward flowing fluid is $p_+(\psi)$, which is shown as the broken line on Fig. 7. On the plane of symmetry, inflowing and outflowing fluid are indistinguishable: hence $p_+(\psi) = 1/2\, p(\psi)$. As η increases, $p_+(\psi)$ is biased towards larger values of ψ [compared with $p(\psi)$] since outward flowing fluid comes from regions of higher mean levels.

Figure 8 shows the joint pdf of the radial and circumferential velocities at $\eta = 1.0$. This joint pdf is defined by

$$f_{r\theta}(V_r, V_\theta) = \int\int f(V_r, V_\theta, V_z, \psi)\, dV_z\, d\psi \quad . \tag{34}$$

The figure shows $f_{r\theta}(V_r, V_\theta)$ plotted against V_r for different values of V_θ. At this location ($\eta = 1.0$) the mean circumferential velocity is $\langle U_\theta \rangle = -0.04$, and the mean radial velocity is $\langle U_r \rangle \approx 0.5$. It may be seen that the joint pdf is a maximum close to $V_r = \langle U_r \rangle$, $V_\theta = \langle U_\theta \rangle$. That the curves of $f_{r\theta}(V_r, V_\theta)$ move to higher values of V_r as V_θ

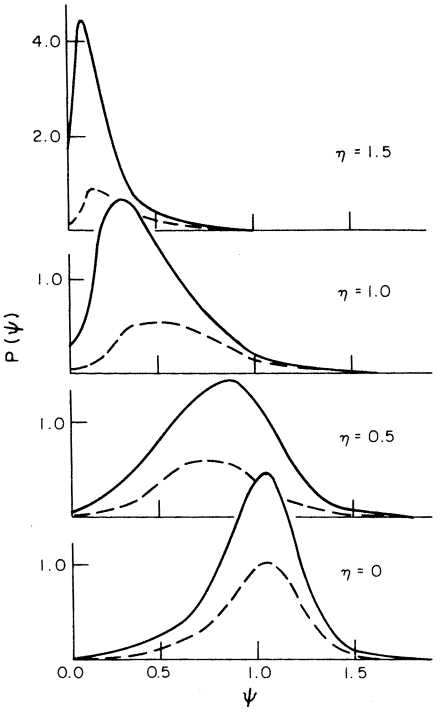

Fig. 7. Scalar pdf's and the contribution from outward-flowing fluid at different lateral positions: (——) $p(\psi)$; (– – –) $p_+(\psi)$

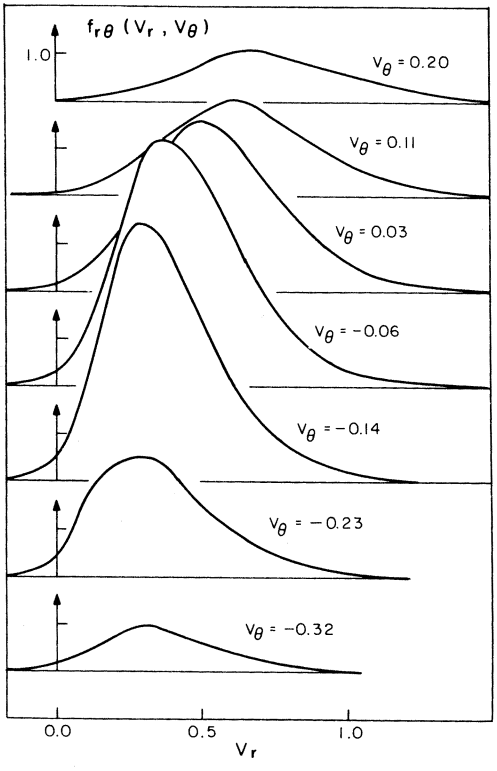

Fig. 8. Joint pdf of radial and circumferential velocity at $\eta = 1.0$

indicates that the shear stress $\langle u_r u_\theta \rangle$ is positive (cf. Fig. 5). For large V_θ ($V_\theta = 0.20$) it may be seen that the distribution is broader than for small values ($V_\theta = 0.32$). This is because the normal stress $\langle u_r^2 \rangle$ is greater for $\eta < 1$, where outward flowing fluid ($V_\theta > 0$) originates.

Figures 7 and 8 illustrate just two quantities that can be obtained from the calculated joint pdf. Any other one-point statistic can also be deduced – for example, conditionally expected values and conditional pdf's.

Conclusion

The velocity-scalar joint pdf transport equation has been solved for the self-similar plane jet. The solution procedure is not computationally expensive even though the joint pdf is a function of five independent variables. In general, there is good agreement between the calculations and measurements.

Acknowledgement. This work was supported in part by grant number CPE8000026 from the National Science Foundation, Engineering energetics program.

References

1. S.B. Pope: Phys. Fluids **24**, 588 (1981)
2. T.S. Lundgren: Phys. Fluids **12**, 485 (1969)
3. C. Dopazo, E.E. O'Brien: Acta Astronaut. **1**, 1239 (1974)
4. S.B. Pope: 18th International Symposium on Combustion, The Combustion Institute (1981)
5. J. Janicka, W. Kolbe, W. Kollmann: Proc. of the Heat Transfer and Fluid Mechanics Institute. Stanford, 1978, p. 296
6. S.B. Pope: Combust. Sci. Technol. **25**, 159 (1981)
7. G. Heskestad: J. Appl. Mech. **32**, 721 (1965)
8. B.E. Launder, G.J. Reece, W. Rodi: J. Fluid Mech. **68**, 537 (1975)
9. J.C. Rotta: Z. Phys. **129**, 547 (1951)
10. R.L. Curl: AIChE J. **9**, 175 (1963)
11. D.B. Spalding: Chem. Eng. Sci. **26**, 95 (1971)
12. P.E. Jenkins, V.W. Goldschmidt: J. Fluids Eng. **95**, 581 (1973)